Journal of Applied Fluid Mechanics, Vol. 10, No. 6, pp. 1639-1648, 2017.
Available online at www.jafmonline.net, ISSN 1735-3572, EISSN 1735-3645.
DOI: 10.18869/acadpub.jafm.73.243.27885

Numerical Simulation of MHD Fluid Flow inside Constricted Channels using Lattice Boltzmann Method

M. Jamali Ghahderijani[1,2], M. Esmaeili[3], M. Afrand[1,2†] and A. Karimipour[1,2]

[1] *Department of Mechanical Engineering, Najafabad Branch, Islamic Azad University, Najafabad, Iran*
[2] *Modern Manufacturing Technologies Research Center, Najafabad Branch, Islamic Azad University, Najafabad, Iran*
[3] *Department of Mechanical Engineering, faculty of Engineering, Kharazmi University, Tehran, Iran.*

†*Corresponding Author Email: masoud.afrand@pmc.iaun.ac.ir*

(Received April 18, 2017; accepted July 9, 2017)

ABSTRACT

In this study, the electrically conducting fluid flow inside a channel with local symmetric constrictions, in the presence of a uniform transverse magnetic field is investigated using Lattice Boltzmann Method (LBM). To simulate Magnetohydrodynamics (MHD) flow, the extended model of D2Q9 for MHD has been used. In this model, the magnetic induction equation is solved in a similar manner to hydrodynamic flow field which is easy for programming. This extended model has a capability of simultaneously solving both magnetic and hydrodynamic fields; so that, it is possible to simulate MHD flow for various magnetic Reynolds number (Re_m). Moreover, the effects of Rem on the flow characteristics are investigated. It is observed that, an increase in Rem, while keeping the Hartman number (Ha) constant, can control the separation zone; furthermore, comparing to increasing Ha, it doesn't result in a significant pressure drop along the channel.

Keywords: Lattice Boltzmann method; Magnetohydrodynamics; Constrictions; Magnetic Reynolds number; Hartmann number.

NOMENCLATURE

a	analytical value	m	average
B	magnetic induction field	P	local pressure
B0	constant transverse magnetic field	Re	Reynolds number
b	simulated Boltzmann value	Re_m	magnetic Reynolds number
BGK	Bhatnagar–Gross–Krook	u	flow velocity
CFD	Computational Fluid Dynamics	w_i	weighted factor indirection i
Cs	sound speed	x_0	location of minimum cross-section
e	lattice velocity in hydrodynamic field	x	cartesian coordinate of x-direction
F	uniform forcing in the along-channel direction	y	cartesian coordinate of y-direction
f	particle mass distribution function		
f_i^{eq}	equilibrium distribution function	δ	constriction height
g	vector distribution function	η	magnetic resistivity
H	channel Height	ρ	local flow density
Ha	Hartmann number	τ	relaxation time
k	constriction width	τ_m	magnetic relaxation time
L	channel Length	v	kinematic viscosity
LBM	Lattice Boltzmann Method	Ξ_j	lattice velocity in magnetic field
MHD	magnetohydrodynamics	Ω_i	collision operator in direction i

1. INTRODUCTION

Flow in constricted channels and tubes are observed in some fluidic devices (orifices, valves) and have wide applications in engineering as well as physiological applications. Because of such industrial and physiological applications, it is of no surprise that flow through local constrictions has been the subject of many studies in the past, in both experimental and numerical domains (Ahmed and Giddens, 1981; Deshpande *et al*., 1976; Lee and Fung, 1970; Neren, 1992; Young, 1979; Giddens *et al*., 1993; Lee, 1994; Chouly and Lagree, 2012; Bandyopadhyay and Layek, 2011; 2012). Such studies have already revealed that normal blood flow can be affected by factors such as wall shear stress, pressure fluctuations, and local velocities (Ahmed and Giddens, 1981; Deshpande *et al*., 1976; Lee and Fung, 1970; Neren, 1992; Young, 1979). The degree of importance of the shape, breadth, and height of the constriction has also been revealed through such studies (Giddens *et al*., 1993; Lee, 1994; Bandyopadhyay and Layek, 2011).

The main objective of previous studies has been to better understand flow irregularities caused by such local constrictions. The Present paper follows another objective which is to see if flow separation occurring downstream a partially-constricted passage can be controlled through the use of an external magnetic field. This idea has been investigated in several studies (Bandyopadhyay and Layek, 2011; Cramer and Pai , 1973; Esmaeili and Sadeghy, 2009; Gad-el-Hak and Bushnell, 1991; Midya *et al*., 2004) especially in biology and medicine (Barnothy, 1964; Vardanyan, 1973; Ponalagusamy and Tamil, 2013; Sinha and Misra, 2012; Ikbal *et al*., 2009; Mustapha *et al*., 2009; Tashtoush and Magableh, 2007; Tzirtzilakis, 2005) but the novelty of current study is the application of a different numerical method for simulation of the mentioned idea.

There are several approaches to numerical simulation of MHD flow (Afrand, 2017; Afrand *et al*., 2015; Afrand *et al*., 2015; Afrand *et al*., 2014; Afrand *et al*., 2014; Afrand *et al*., 2017;). Among them the lattice Boltzmann method (LBM) is a new and popular approach (He and Luo, 1997). In contrast to traditional computational fluid dynamics (CFD) methods which solve Navier–Stokes equations and compute macroscopic variables such as velocity and pressure in the LBM the particle mass distribution function f on the mesoscopic level is obtained by an approximation of the kinetic equation using the lattice Boltzmann equation (Mei *et al*., 1999). Then macroscopic variables are computed by this mass distribution function.

The simplicity and suitability for parallel programming have made the lattice Boltzmann algorithms so popular. In addition, they can be easily incorporated for simulating fluid flows on complex geometries with complicated boundary conditions (Agarwal *et al*., 2009). Among several LBM algorithms the Bhatnagar–Gross–Krook (BGK) model with a simple scalar relaxation parameter and mass distribution function is the simplest one. In recent years the LBGK model for MHD flow has been developed. The earlier LBGK model in this area was presented by Chen *et al*. (1991). This model was an extension of lattice gas cellular automata MHD proposed by Chen and Matthaeus, 1987 and Chen *et al*., 1988. In their model, a two-index particle distribution function was used corresponding to separate microscopic velocities for velocity and magnetic field. At streaming step each particle moves along with one of the two velocity vectors which are chosen randomly. Martinez *et al*. (1994) have proposed another model which reduces the number of necessary particle states and computation effort as a result. Bouchut (1999) has introduced a vector-valued distribution function instead of the scalar probability distribution function. Dellar (2002) has also characterized an approach based on Bouchut model. In this model a separate vector-valued magnetic distribution function based on a vector Boltzmann–BGK equation gives the magnetic field. This model can solve induction equation in a manner similar to fluid flow so it is appropriate for programming. The model proposed by Dellar (2002) has been used in the current study.

The paper has been organized as follows: we will start by presenting the computational domain which is laminar, incompressible fluid flow between two parallel plates containing a Gaussian symmetric, local constriction. It is also assumed that the fluid flow temperature is constant. We will then proceed with describing the lattice Boltzmann method as the method of solution. The magnetic induction equations which can be solved in a similar manner to the hydrodynamic equations (using a vector distribution function) are described next in details. Typical numerical results will be presented demonstrating magnetic field effects on flow characteristics in constricted channels. The paper is concluded with presenting a brief summary of the main findings of the work.

2. METHOD AND SIMULATION

We consider laminar flow of an electrically conducting fluid flow between two parallel plates having an overall length of L which are separated by a distance 2H from each other (see Fig. 1). As can be seen in Fig. 1, there is a local symmetric constriction somewhere between the two plates; it is seen to have amplitude of δ (constriction height) and a span of 4k (constriction width). The shape of constriction, assumes to be Gaussian type; that is

$$y = H - \delta \exp\left[-\left(\frac{x - x_0}{k}\right)^2\right] \tag{1}$$

In Eq. (1) x_0 is the location of minimum cross-section (at the throat of channel).

In this paper we assumed that the minimum cross-section is located in the middle of channel. Also, the ratio of channel length (L) to channel height (2H) is 16. For simulation electrically conducting fluid flow through constricted channel (above mentioned geometry) the LBM is used which is

discussed in the following section.

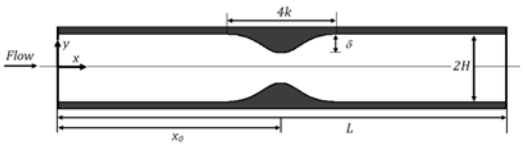

Fig. 1. Schematic showing the constricted channel shape used in the present study.

2.1 Lattice Boltzmann Method

The LBM is a numerical scheme in mesoscopic scale which solves the LB equation for obtaining macroscopic flow field properties. Alternatively, this method can be used to simulate complex flow and transport phenomena especially in cases where direct solution of Navier-Stokes equations is not feasible (Martinez *et al.*, 1994; Bouchut, 1999; Dellar, 2002). The LBM has already been successfully used in various fluid flow problems, such as multiphase and multicomponent fluid flows (Bao and Schaefer, 2012; Yan *et al.*, 2011), thermal flow (Attar and Körner, 2011; Chen *et al.*, 2012; Lin *et al.*, 2012; Rong *et al.*, 2010), flows through porous media (Rong *et al.*, 2010; Hirabayashi *et al.*, 2012; Boek and Venturoli, 2010), solid particle suspensions (Hirabayashi *et al.*, 2012), non-Newtonian fluids (Chai *et al.*, 2011; Ohta *et al.*, 2011), reaction diffusion systems (Bresolin and Oliveira, 2012), and magneto-hydrodynamics, (Chen *et al.*, 1991; Chen and Matthaeus, 1987; Chen *et al.* 1988; Martinez*et al.*, 1994; Bouchut, 1999; Dellar, 2002;2011; Kefayati *et al.*, 2012).

To conserve mass and momentum and ensuring that the fluid is isotropic, in the LBM the particle distribution functions, fi(x, t) at a point x and time t, move synchronously on a regular lattice (Boyd and Buick, 2007). Fig. 2 shows the D2Q9 lattice model used in this paper. Only the five speeds 0, 1, 2, 3, 4, shown with thick lines, are used for the magnetic field. The distribution functions are given by the Lattice Boltzmann equation (Chen and Doolen, 1998):

$$f_i\left(x+e_i\Delta t,t+\Delta t\right)=f_i\left(x,t\right)+\Omega_i\left(x,t\right) \tag{2}$$

Where in the case of D2Q9 lattice

$$e_0=(0,0);\ \ (i=0) \tag{3}$$

$$e_i=\left[\cos\left(\frac{\pi}{2}(i-1)\right),\sin\left(\frac{\pi}{2}(i-1)\right)\right];\ (i=1,2,3,4) \tag{4}$$

$$e_i=\sqrt{2}\left[\cos\left(\frac{\pi}{2}(i-1)+\frac{\pi}{4}\right),\sin\left(\frac{\pi}{2}(i-1)+\frac{\pi}{4}\right)\right];\ (i=5,6,7,8) \tag{5}$$

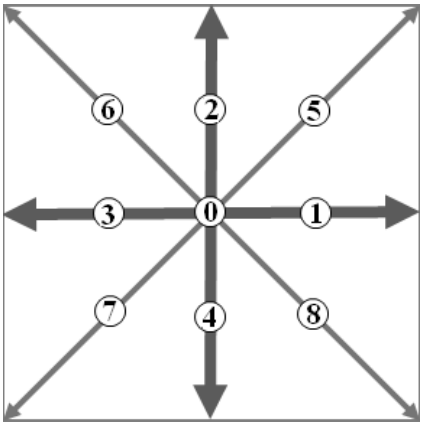

Fig. 2. The D2Q9 lattice model for MHD flow.

The collision operator Ω is given by the Bhatnagar–Gross–Krook approximation (Ohta *et al.*, 2011; Bhatnagar *et al.*, 1954):

$$\Omega_i=-\frac{1}{\tau}\left[f_i(x,t)-f_i^{eq}(x,t)\right] \tag{6}$$

In the above equation τ is a relaxation time and f_i^{eq} is the equilibrium distribution function given by the local fluid density, ρ, and flow velocity, u, as follows:

$$f_i^{eq}(x)=w_i\rho(x)\left[1+3e_iu+\frac{9}{2}(e_iu)^2-\frac{3}{2}u^2\right] \tag{7}$$

Where the weight factors w_i are as below:

w_i=4/9	i=0 (the rest particles)
w_i=1/9	i=1, 2, 3, 4
w_i=1/36	i = 5, 6, 7, 8

In this model an ideal gas equation of state is used (i.e. $P=\rho c_s^2$) where $c_s^2=1/3$ is the speed of sound.

The fluid density ρ and velocity u can be easily obtained by $\rho=\sum_i f_i$ and $\rho u=\sum_i f_i e_i$, respectively at each node. It is worth mentioning that the kinematic viscosity can be expressed by $\upsilon=(2\tau-1)/6$.

2.2 Magnetohydrodynamics Approach

Calculation of the magnetic field in MHD flow can be done using the magnetic induction equation (Moreau, 1990):

$$\frac{\partial B}{\partial t}+\nabla.(uB-Bu)=\eta\nabla^2B \tag{8}$$

Where B and η represent magnetic induction field and magnetic resistivity, respectively. The magnetic induction equation can be solved in a similar manner to the hydrodynamic equations, using a vector distribution function, g. The evolution of this function is given by (Dellar, 2002)

$$g_{i\beta}\left(x+\Xi_i\Delta t,t+\Delta t\right)=g_{i\beta}\left(x,t\right)-\frac{1}{\tau_m}\left[g_{i\beta}\left(x,t\right)-g_{i\beta}^{eq}\left(x,t\right)\right] \quad (9)$$

$$g_{i\beta}^{eq}=W_i\left[B_\beta+3\Xi_{i\alpha}\left(u_\alpha B_\beta-B_\alpha u_\beta\right)\right] \quad (10)$$

$$B_\alpha=\sum_{i=0}^{4}g_{ia} \quad (11)$$

Where Ξ_i is lattice velocity in magnetic field and τ_m is magnetic relaxation time. The five-point lattice weight factors W_i used for magnetic field are as below:

W_i=1/3 i=0 (the rest particles)

W_i=1/6 i=1, 2, 3, 4

In two space dimensions the magnetic resistivity is related to the magnetic relaxation time by $\eta=(2\tau_m-1)/6$. Assuming $B = (B_x , B_y , 0)$, a suitable equilibrium distribution is

$$f_i^{eq}\left(x\right)=w_i\rho\left(x\right)\left[1+3e_iu+\frac{9}{2}\left(e_iu\right)^2-\frac{3}{2}u^2\right]+\frac{9}{2}w_i\left[\frac{1}{2}\left|B\right|^2\left|e_i\right|^2-\left(e_iB\right)^2\right] \quad (12)$$

It is worth mentioning that the velocity field is coupled with magnetic field using above equation. To solve the governing equations, we need to impose suitable boundary conditions. At the inlet we impose fully developed velocity profile (Eq. (15) for MHD problem and a Poiseuille velocity profile for Ha=0) according to Zou and He (1997) method. Also, for solid walls a mid-grid bounce back boundary condition (Succi , 2001) is used. For the magnetic boundary conditions, the bounce-back method is also used, but with the sign reversed to enforce Bx = 0 at the wall boundaries (Dellar, 2002).

At the outlet, we assume that the downstream exit length is chosen long enough so that the flow streamwise variations in the flow will become sufficiently small. As a result the zero-derivative boundary conditions can be applied. This zero gradient condition is based on linear extrapolation (Kefayati *et al*., 2012), as follows:

$$f_i\left(x,t+e_i\Delta t\right)=2f_i\left(x+e_i\Delta t,t+\Delta t\right)-f_i\left(x+2e_i\Delta t,t+\Delta t\right) \quad (13)$$

2.3 Hartmann Flow

Hartmann flow comprises a steady unidirectional flow of viscous, electrically conducting fluid through a channel containing a constant transverse magnetic field. The fluid, assumed incompressible and all relevant quantities, except the pressure, are a function of only the transverse coordinate, u = (u(y), 0, 0), B = (Bx(y), B0, 0) where B0 is the constant magnetic field transverse to the channel length. A uniform and time independent pressure gradient is maintained along the channel direction to drive the fluid. The walls are located at y = − H and y = H (Martinez *et al*., 1994). For this case, the incompressible MHD equations can be simplified to the following linear system (Dellar, 2002)

$$F+\rho_0\upsilon\frac{d^2u}{dy^2}+B_0\frac{dB}{dy}=0$$
$$B\frac{du}{dy}+\eta\frac{d^2B}{dy^2}=0 \quad (14)$$

In the above equation F is spatially uniform force acting along channel direction, such as a pressure gradient. There is an analytical solution for Eq.14 if non-slip boundary conditions is applied for the velocity field and accompanied by B_x (−H) = B_x (H) = 0 for the magnetic field.

$$B(y)=\frac{FH}{B_0}\left(\frac{\sinh\left(Ha\,y/h\right)}{\sinh\left(Ha\right)}-\frac{y}{H}\right)$$
$$u(y)=\frac{FH}{\sqrt{\rho B_0}}\sqrt{\frac{\eta}{\upsilon}}\coth\left(Ha\right)\left(1-\frac{\cosh\left(Ha\,y/h\right)}{\cosh\left(Ha\right)}\right) \quad (15)$$

where Ha is a dimensionless Hartmann number which represents the ratio of Lorentz force to viscous force and can be defined by $Ha=B_0H/\sqrt{\rho_0\eta\upsilon}$.

When the Hartmann number is large, as is typical in liquid metal MHD applications, the magnetic field maintains a nearly uniform velocity u over the bulk of the channel (Dellar, 2002). Conversely, for zero Hartmann number which means no external magnetic field the solution will reduce to the parabolic velocity profile of the Poiseuille flow.

3. VALIDATION

To examine the validity of the code, the obtained velocity profile and axial component of induced magnetic field, B_x, in a straight channel are compared with analytical solution of Eq. (15) (see Fig. 3). The Reynolds number and magnetic Reynolds number defined by $\mathrm{Re}=U_mH/\upsilon$ and $\mathrm{Re_m}=U_mH/\eta$ where U_m denotes average velocity at inlet of the channel and η denotes magnetic resistivity.It is assumed that the Reynolds number and magnetic Reynolds number are constant (Re=50, $\mathrm{Re_m}$=5) along different Hartmann numbers. To reduce compressibility error inlet Mach number ($\mathrm{Ma_{in}}=U_m/C_s$) set to be equal to 0.026.

For any given flow rate, a decrease in the velocity near the centerline must be accompanied by an increase in the velocity near the walls, as can be inferred from Fig. 3a. Moreover, in Fig. 3b the axial component of induced magnetic field grows from zero on the wall to its maximum adjacent to the surface and then experiencing a point of inflection once again falls to zero in the centerline. The mentioned maximum value decreases with increasing Ha number.

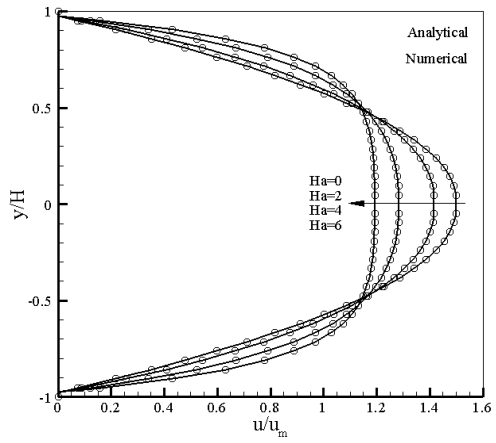

(a)

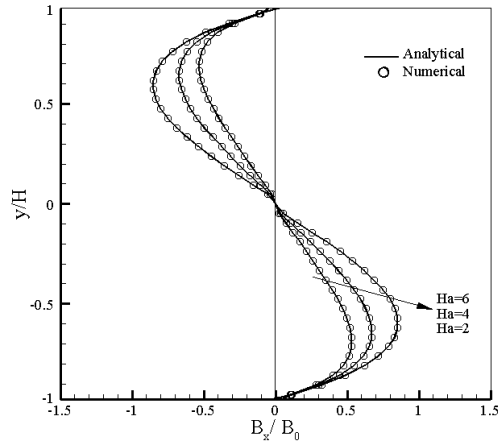

(b)

Fig. 3. Comparison between analytical and numerical results of (a)Velocity profile and (b) induced magnetic field profiles.

It is worth mentioning that a good agreement is observed between numerical results and analytical solutions. The second order accuracy of MHD Lattice Boltzmann method (Dellar, 2002) was also investigated. The simulations were finished when the following criterion was satisfied.

$$\sum_x \left\| u(x,t) - u(x,t-1) \right\| < \varepsilon \tag{16}$$

where ε is a small number assumed to be $\varepsilon=1\times10^{-10}$. The global error can be calculated by Eq. (17).

$$\zeta = \frac{\dfrac{\sum_x \left\| u_b(y) - u_a(y) \right\|}{\sum_x \left\| u_a(y) \right\|}}{\dfrac{\sum_x \left\| B_b(y) - B_a(y) \right\|}{\sum_x \left\| B_a(y) \right\|}} \tag{17}$$

In the Eq.17 the subscript *a*, denotes results of the exact analytic solution while the subscript *b* refers to the obtained results from LBM simulation. Results for the global error have been shown in Fig. 4. The black lines in Fig. 4 represent lines of slope −2, indicating second-order behavior. Although, the amount of error for axial magnetic field is higher than velocity field, it can be seen that for various Hartmann number the presented data closely match the slope of those lines. These results prove that the code can well represent MHD flow in channels.

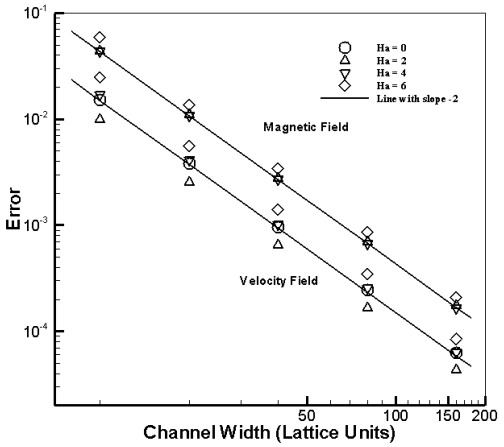

Fig. 4. Global error for MHD Lattice Boltzmann Method.

4. RESULTS AND DISCUSSION

Having found the fully-developed velocity profiles in the previous section, one can proceed with calculating the velocity profiles in the constriction region. To achieve this goal, we used a uniform grid consisting 125 nodes along the channel height and 2000 nodes along the channel length. To produce various Reynolds number, we changed viscosity, ν, so that the relaxation time would be changed too. For Re=50 the relaxation time, τ , and the inlet Mach number, Ma_{in} is set to be 0.5562 and 0.026 respectively. To perform various magnetic Reynolds number, Re_m, the magnetic resistivity, η, was changed. For Re_m=5, magnetic relaxation time is set to be 1.0625.

Figure 5 illustrates the effect of the constriction height, δ, on the streamwise velocity profile at x/H=17 (i.e., downstream the throat), a constriction with k/H=0.4 for Re=50 and Ha=0. The negative values of the velocity imply the recirculating flow region. As the height of the constriction increases the greater separation zone in the upper and lower walls of the channel can be observed.

Figure 6 shows a history of the development of the streamlines inside a constricted channel (with δ/H=0.5 and k/H=0.4.) for Ha=0 at Re=25, 50 and 75.). A flow reversal (i.e., separation) downstream of the throat is obvious in this figure. Evidently, once the flow enters the diverging section of the channel, it is vulnerable to separation because of the influence of the adverse pressure gradient in this part of the channel. As expected, separated zone grows further with the increase of Reynolds number (the inertia forces become more important than the viscous forces), and at Re=75 (Fig .6c) it occupies

main portion of the channel.

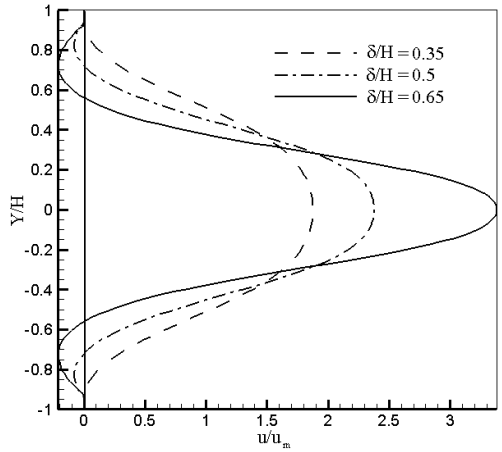

Fig. 5. Effect of constriction height,δ , on the velocity profiles at x/H = 17 for Re=50 and Ha=0.

Here, the effect of Hartman number on the velocity profile at x/H= 17, Re=50 and Re_m=5 for a constriction with δ/H=0.5 and k/H=0.4 is investigated.

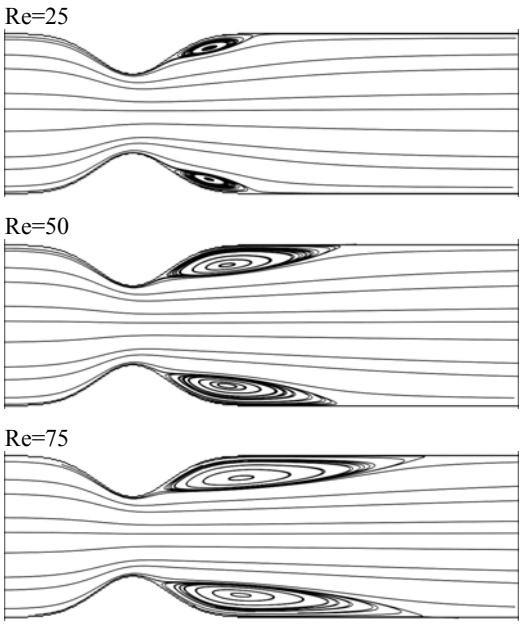

Fig. 6. Streamline pattern at various Reynolds number, Re, at Ha=0.

As can be observed in Fig. 7, the Lorentz force, as induced by the magnetic field, is predicted to have a retarding effect on fluid elements near the axis of the constriction. Close to the wall, however, fluid elements accelerate to keep the mass flow rate constant. This increase in the fluid velocity near the walls with increasing Ha number enables the fluid to overcome the influence of any adverse pressure gradient (downstream of the constriction) and thereby enhances the ability of the fluid to withstand flow separation near the wall.

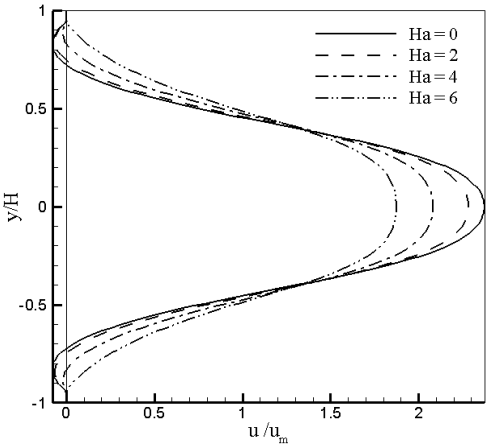

Fig. 7. Velocity profiles at various Hartman number for x/H = 17, Re=50 and Re_m=5.

The effect of Hartman number on the streamline pattern is shown in Fig. 8. As can be seen in this figure, with an increase in the magnetic field, the flow separation zone becomes smaller in size and for greater Hartman numbers; the separation zone is vanished totally. These results are in line with the velocity profiles presented in Fig. 7. Evidently, the accelerating effect of the magnetic field (through the action of the Lorentz force) can compensate for the decelerating effect of the adverse pressure gradient near the wall and downstream the throat more.

Table1 Effect of Hartmann number on the overall wall friction

Ha	$\overline{C_f}$.Re
0	6.195621
2	6.859182
4	9.889191
6	13.14766
straight channel	6

The effect of Hartmann number on overall wall friction (it can be obtained with integrating of C_f.Re on the wall surface) is summarized in Table 1. It is clear from this table that the overall wall friction increases with an increase in the strength of magnetic field. An increase of the wall friction with an increase of the Hartman number can be attributed to the boundary layer becoming thinner due to the higher Hartman number resulting in an increase in the velocity gradient near the wall (see Fig .3a).

Figure 9 reperesents the effect of Hartman number on the pressure variation for Re=50 and Re_m=5. It is concluded from this figure that by increasing the Hartmann number from 0 to 6, the pressure drop increases dramatically. This result is attributed to increase of wall shear stress due to the increase of velocity gradient near the wall. In this connection it is important to mention that since in the real situations the externally applied pressure gradient will need to be adjusted appropriately, we cannot

strictly conclude that more increase in Ha number is a completely effective way to cause a delay in separation.

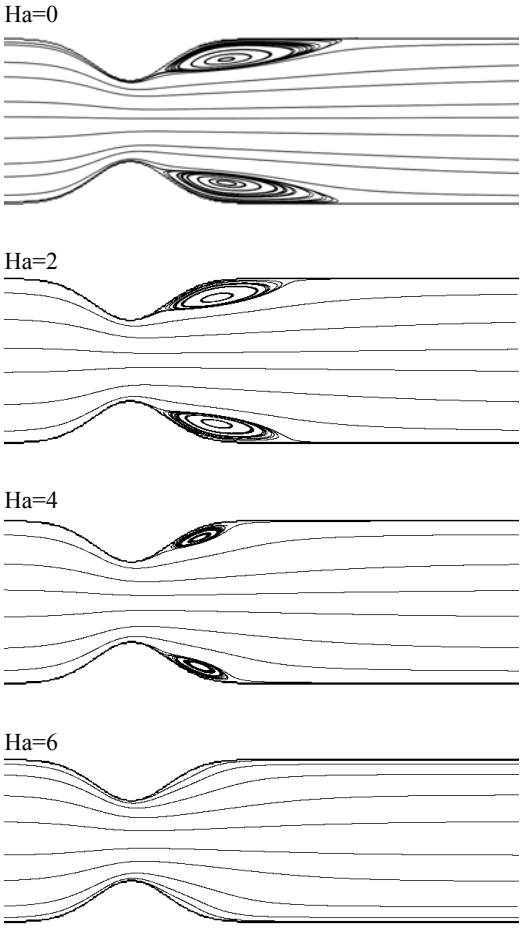

Fig. 8. Streamline pattern at various Hartmann number, Ha, for Re=50 and Re_m=5.

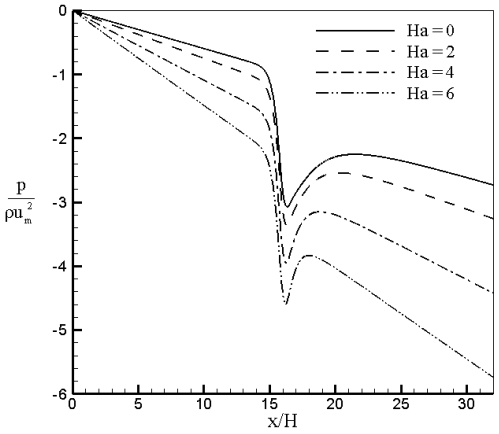

Fig.9. Effect of the Hartmann number, Ha, on the dimensionless pressure at the axis of channel Re=50 and Re_m=5.

Figure 10 shows the effect of magnetic Reynolds number on streamline patterns at constant Hartmann number (Ha=2). It can be seen that, by increasing the magnetic Reynolds number from 5 to 150, the diffusion term in Eq. (8) decreases (because of the magnetic resistivity, η, reduction) and convection term becomes more important. As a result, the induced magnetic field increases in comparison with the uniform transverse magnetic field and the separation zone becomes smaller in size. In Fig. 11 the variation of magnetic Reynolds number with stream wise velocity is depicted at x/H= 17. This confirms that, similar to Hartmann number, Re_m has an increasing effect on velocity of fluid elements close to the wall. However, as can be seen in Fig. 12 the pressure drop due to increasing magnetic Reynolds number is not significant. In fact, increasing Re_m just results in increasing induced magnetic field in the constrictions region which accelerates fluid flow near wall. So, flow doesn't have to tolerate large velocity gradient on the wall along the whole channel length which causes considerably less pressure drop.

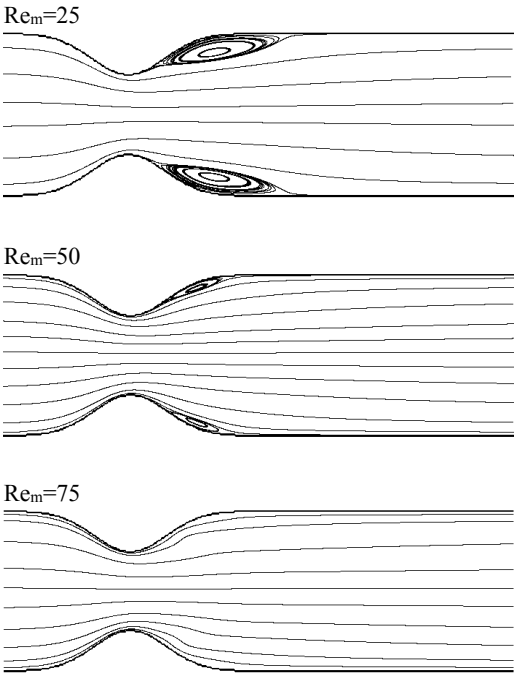

Fig. 10. Streamline pattern at various magnetic Reynolds number, Rem, for Re=50 and Ha=2.

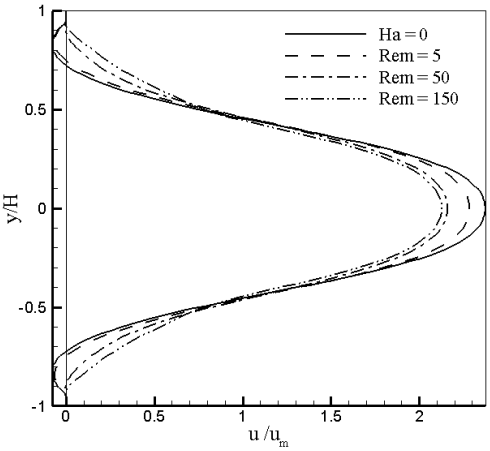

Fig. 11. Velocity profiles at various magnetic Reynolds number for x/H = 17 and Re=50.

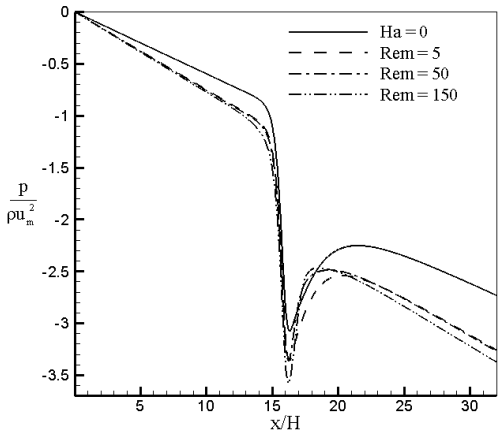

Fig. 12. Effect of the Magnetic Reynolds number, Re_m, on the dimensionless pressure at the axis of channel Re=50 and Ha=2.

5. CONCLUSION

In this paper, numerical simulation of electrically conducting fluid flow inside a locally constricted channel using lattice Boltzmann method is investigated. Simultaneously solving magnetic and hydrodynamic fields, makes it possible to study the effect of various magnetic Reynolds number in the simulation. It is observed that flow separates at the lee of constriction and this separated zone will be larger when the Reynolds number increases. To control flow separation, two scenarios are suggested which include increasing Ha and Re_m. It is viewed that increasing Ha can reduce the separated zone in downstream of constrictions whereas considerable pressure drop along channel length occurs. However, while Ha is kept constant, an increase in Re_m not only could delay the separation phenomena but also significant pressure drop does not occur.

ACKNOWLEDGMENT

The authors would like to express their sincere gratitude to Mr. Hassan Barzegar Aval and Dr. Reza Haghighi for their constructive comments and helpful suggestions.

REFERENCES

Afrand, M. (2017). Using a magnetic field to reduce natural convection in a vertical cylindrical annulus. *International Journal of Thermal Sciences* 118(1), 12-23.

Afrand, M., S. Farahat, A. Hossein Nezhad, G. A. Sheikhzadeh, F. Sarhaddi and S. Wongwises (2015). Multi-objective optimization of natural convection in a cylindrical annulus mold under magnetic field using particle swarm algorithm. *International Communications in Heat and Mass Transfer* 60(1), 13-20.

Afrand, M., S. Farahat, A. Hossein Nezhad, G. A. Sheikhzadeh and F. Sarhaddi (2014). 3-D numerical investigation of natural convection in a tilted cylindrical annulus containing molten potassium and controlling it using various magnetic fields. *International Journal of Applied Electromagnetics and Mechanics* 46(4), 809-821.

Afrand, M., S. Farahat, A. Hossein Nezhad, G. A. Sheikhzadeh and F. Sarhaddi (2014). Numerical simulation of electrically conducting fluid flow and free convective heat transfer in an annulus on applying a magnetic field. *Heat Transfer Research* 45(8), 749-766.

Afrand, M., S. Rostami, M. Akbari, S. Wongwises, M. H. Esfe and A. Karimipour (2015). Effect of induced electric field on magneto-natural convection in a vertical cylindrical annulus filled with liquid potassium. *International Journal of Heat and Mass Transfer* 90(1), 418-426.

Afrand, M., D. Toghraie, A. Karimipour and S. Wongwises (2017). A Numerical Study of Natural Convection in a Vertical Annulus Filled with Gallium in the Presence of Magnetic Field. *Journal of Magnetism and Magnetic Materials* 430(1), 22–28.

Agarwal, R., L. Chusak and B. Morgan (2009). Lattice Boltzmann Simulations of Slip Flow of Newtonian and Non-Newtonian Fluids in Microgeometries. *47th AIAA Aerospace Sciences Meeting*, Orlando, Florida 1119-1129.

Ahmed, S. and D. Giddens (1981). Velocity measurements in steady flow through axisymmetric stenoses at moderate Reynolds numbers. *Journal of Biomechanics* 16(7), 505-516.

Attar, E. and C. Körner (2011). Lattice Boltzmann model for thermal free surface flows with liquid–solid phase transition. *International Journal of Heat and Fluid Flow* 32(1), 156–163.

Bandyopadhyay, S. and G. C. Layek (2011). Numerical computation of pulsatile flow through a locally constricted channel. *Communications in Nonlinear Science and Numerical Simulation* 16(1), 252–265.

Bandyopadhyay, S. and G. C. Layek (2012). Study of magnetohydrodynamic pulsatile flow in a constricted channel. *Communications in Nonlinear Science and Numerical Simulation* 17(6), 2434–2446.

Bao, J. and L. Schaefer (2012). Lattice Boltzmann equation model for multi-component multi-phase flow with high density ratios. *Applied Mathematical Modelling* 37(4), 1860–1871.

Barnothy, M. (1964). Biological Effects of Magnetic Fields, *Plenum Press*, New York

Bhatnagar, P. L., E. P. Gros and M. Krook (1954). A model for collision processes in gases. I. Small amplitude processes in charged and neural one-component systems. *Physical Review* 94(3), 511-525.

Boek, E. and M. Venturoli (2010). Lattice-

Boltzmann studies of fluid flow in porous media with realistic rock geometries. *Computers and Mathematics with Applications* 59(7), 2305-2314.

Bouchut, F. (1999). Construction of BGK models with a family of kinetic entropies for a given system of conservation laws. *Journal of Statistical Physics* 95(1-2), 113- 170.

Boyd, J. and J. Buick (2007). Comparison of Newtonian and non-Newtonian flows in a two-dimensional carotid artery model using the lattice Boltzmann model. *Physics in Medicine and Biology* 52(20), 6215-6228.

Bresolin, C. and A. Oliveira (2012). An algorithm based on collision theory for the lattice Boltzmann simulation of isothermal mass diffusion with chemical reaction. *Computer Physics Communications* 183(12), 2542–2549.

Chai, Z., B. Shi, Z. Guo and F. Rong (2011). Multiple-relaxation-time lattice Boltzmann model for generalized Newtonian fluid flows. *Journal of Non-Newtonian Fluid Mechanics* 166(5-6), 332–342.

Chen, S., K. Luo and C. Zheng (2012). A simple enthalpy-based lattice Boltzmann scheme for complicated thermal systems. *Journal of Computational Physics* 231(24), 8278–8294.

Chen, H. and W. Matthaeus (1987). New cellular automaton model for magnetohydrodynamics. *Physical Review Letters* 59(1), 1845-1848.

Chen, H., W. Matthaeus and L. Klein (1988). An analytic theory and formulation of a local magnetohydrodynamic lattice gas model. *Physical Review Letters* 31(6), 1439-1455.

Chen, S. and G. Doolen (1998). Lattice Boltzmann method for fluid flows. *Annual Review of Fluid Mechanics* 30(1): 329-364.

Chen, S., H. Chen, D. Martınez and W. Matthaeus (1991). Lattice Boltzmann Model for simulation of Magnetohydrodynamics. *Physical Review Letters* 67(27), 3776-3779.

Chouly, F. and P. Lagree, (2012). Comparison of computations of asymptotic flow models in a constricted channel. *Applied Mathematical Modelling* 36(12), 6061–6071.

Cramer, K. and S. Pai (1973). Magnetofluid dynamics for engineers and applied physicists. *Scripta Publishing Company*, Washington, DC.

Dellar, P. (2002). Lattice Kinetic Schemes for Magnetohydrodynamics. *Journal of Computational Physics* 179(1), 95-126.

Dellar, P. (2011). Lattice Boltzmann formulation for Braginskii magnetohydrodynamics. *Computers and Fluids* 46(1), 201–205.

Deshpande, M., D. Giddens and R. Mabon (1976). Steady laminar flow through modeled vascular stenosis. *Journal of Biomechanics* 9(4), 165-174.

Esmaeili, M., and K. Sadeghy (2009). MHD Flow of Power-Law Fluids in Locally-Constricted Channels. *Journal of the Society of Rheology* 37(4), 181-189.

Gadel Hak, M. and D. Bushnell (1991). Separation Control: Review. *ASME Journal of Fluids Engineering* 113(1), 5–30.

Giddens, D., C. Zarins and S. Glagov (1993). The role of fluid mechanics in the localization and detection of atherosclerosis. *ASME Journal of Biomechanical Engineering* 115(4B), 588-594.

He, X. and L. Luo (1997). Lattice Boltzmann model for the incompressible Navier-Stokes equation. *Journal of Statistical Physics* 88(3/4), 927-944.

Hirabayashi, S., T. Sato, K. Mitsuhori and Y. Yamamoto (2012). Microscopic numerical simulations of suspension with particle accumulation in porous media. *Powder Technology* 225(143), 143–148.

Ikbal, M., S. Chakravarty, K. Wong, J. Mazumdar and P. Mandal (2009). Unsteady response of non-Newtonian blood flow through a stenosed artery in magnetic field. *Journal of Computational and Applied Mathematics* 230(1), 243–259.

Kefayati, G., M. Gorji-Bandpy, H. Sajjadi and D. Ganji (2012). Lattice Boltzmann simulation of MHD mixed convection in a lid-driven square cavity with linearly heated wall. *Scientia Iranica B* 19(4), 1053–1065.

Lee, J. and Y. Fung (1970). Flow in locally-constricted tubes at low Reynolds numbers. *ASME Journal of Applied Mechanics* 37(1), 9-16.

Lee, T. (1994). Steady Laminar Fluid Flow through a Variable Constriction in Vascular Tube. *ASME Journal of Fluids Engineering* 116(1), 66–71.

Lin, K., C. Liao, S. Lien and C. Lin (2012). Thermal lattice Boltzmann simulations of natural convection with complex geometry. *Computers and Fluids* 69(35), 35–44.

Martinez, D., S. Chen and W. Matthaeus (1994). Lattice Boltzmann Magnetohydrodynamics. *Physics of Plasmas* 1(6), 1850-1894.

Mei, R., L Luo and W. Shyy (1999). An Accurate Curved Boundary Treatment in the Lattice Boltzmann Method. *Journal of Computational Physics* 155(2), 307-330.

Midya, C., G. C. Layek, A. S. Gupta and T. Ray Mahapatra (2004). Magnetohydrodynamic Viscous Flow Separation in a Channel with Constrictions. Journal of Fluids Engineering 125(6), 952-962.

Moreau, R. (1990). Magnetohydrodynamics. *Kluwer Academic Publications*, Dordrecht, Netherlands.

Mustapha, N., N. Amina, S. Chakravarty and P.

Mandal (2009). Unsteady magnetohydrodynamic blood flow through irregular multi-stenosed arteries. *Computers in Biology and Medicine* 39(10), 896–906.

Neren, R. (1992). Vascular fluid mechanics, the arterial wall and atherosclerosis. *ASME Journal of Biomechanical Engineering* 114(3), 274-282.

Ohta, M., T. Nakamura and Y. Yoshida (2011). Lattice Boltzmann simulations of viscoplastic fluid flows through complex flow channels. *Journal of Non-Newtonian Fluid Mechanics* 166(7-8), 404–412.

Ponalagusamy, R. and S. Tamil (2013). Blood flow in stenosed arteries with radially variable viscosity, peripheral plasma layer thickness and magnetic field. *Meccanica* 48(10), 2427–2438.

Rong, F., Z. Guo, Z. Chai and B. Shi (2010). A lattice Boltzmann model for axisymmetric thermal flows through porous media. *International Journal of Heat and Mass Transfer* 53(23-24), 5519–5527.

Sinha, A. and J. C. Misra (2012). Numerical study of flow and heat transfer during oscillatory blood flow in diseased arteries in presence of magnetic fields. *Applied Mathematics and Mechanics* 33(5), 649-662.

Succi, S. (2001) The Lattice Boltzmann equation for Fluid Dynamics and Beyond. *Oxford Univesrity Press Inc*, Oxford, United Kingdom.

Tashtoush, B. and A. Magableh (2007). Magnetic field effect on heat transfer and fluid flow characteristics of blood flow in multi-stenosis arteries. *Heat and Mass Transfer* 44(3), 297-304.

Tzirtzilakis, E. (2005). A mathematical model for blood flow in magnetic field. *Physics of Fluids* 17(7), 077103-077117.

Vardanyan, V. (1973). Effect of Magnetic Field on Blood Flow. *Biofizika* 18(3), 491–496.

Yan, Y., , Y. Zu and B. Dong (2011). LBM, a useful tool for mesoscale modelling of single-phase and multiphase flow. *Applied Thermal Engineering* 31(5), 649-655.

Young, D. (1979). Fluid mechanics of arterial stenoses. *ASME Journal of Biomechanical Engineering* 101(3), 157-175.

Zou, Q. and X. He (1997). On pressure and velocity boundary conditions for the lattice Boltzmann BGK model. *Physics of Fluids* 9(6), 1591-1598.